Effects of grain growth on dynamic surface scaling during the deposition of Al polycrystalline thin films

Adriana E. Lita and John E. Sanchez, Jr.
Department of Materials Science and Engineering, University of Michigan, Ann Arbor, Michigan 48109-2136

(Received 9 August 1999)

Evolution of surface structure during the growth of sputter-deposited polycrystalline Al films is studied by means of atomic force microscopy and dynamic scaling by power spectral density and image variography analyses. We incorporate the effects of grain growth based on quantitative measurements of grain size, morphology, and texture orientation through transmission electron microscopy and x-ray diffraction pole figure texture measurements. Temporal regimes of early surface smoothing followed by roughening are explained by the effects of grain-boundary grooves and grain growth during deposition. Three distinct surface morphologies described as flat grains, hillocks, and ridges develop during film growth. The ridges are periodic structures with constant spacing during growth that form along ⟨110⟩ directions on vicinal (111)-oriented grains and are due to spontaneous development and growth of steps along ⟨110⟩ directions induced by the Schwoebel-barrier mechanism. The spacing of ridge structures and the well-characterized median grain size correspond to characteristic dimensions that define transitions between regimes of combinations of physical processes responsible for surface evolution. We found a surface-diffusion-dominated anomalous scaling growth mode ($\alpha > 1$) at short length scales and a nonlinear KPZ type mode ($\alpha \approx 0.35$) at longer length scales.

INTRODUCTION

There is significant interest in the structure of deposited metal thin films due to their wide application as critical components in electronic, magnetic, and optical devices. The functionality of these films is determined by their physical structure, which includes surface roughness, and, in the case of polycrystalline films, grain-size distribution and crystallographic orientation. Combined characterizations of surface and microstructure may therefore provide an improved mechanistic understanding of the processes driving the physical evolution during film formation. For example, the surfaces of growing films often exhibit apparently irregular geometries that can be analyzed in terms of the scaling properties of the surface fluctuations.[1] The dynamical scaling behavior of a growing surface with evolution in both vertical roughening and lateral scaling arises from the competition between various roughening and smoothing mechanisms. A large number of studies[2–6] have helped to provide understanding of possible mechanisms that generate surface roughness. Theoretical studies based on continuum and discrete growth models have provided scaling relations between roughness (defined as the root-mean-square surface fluctuation R_{rms}) and time (or film thickness) for a growing interface as well as the roughness dependence of the spatial scale of observation in the experiment. Surface structures that preserve a similar morphology upon a change of magnification and a rescaling of the third dimension (z axis) are termed self-affine and play a central role in the theories of growth. For a self-affine growing surface, the roughness can be expressed[6] in the following form:

$$R_{\mathrm{rms}}(L,t) = L^{\alpha} f(t/L^{z}), \tag{1}$$

which can be reduced to

$$R_{\mathrm{rms}}(L,t) \sim t^{\beta} \quad \text{for } t/L^{z} \ll 1, \tag{2}$$

$$R_{\mathrm{rms}}(L,t) \sim L^{\alpha} \quad \text{for } t/L^{z} \gg 1, \tag{3}$$

where L is the length over which the roughness is measured, t is the elapsed time of growth (usually proportional to the amount of material deposited), α is the spatial scaling exponent, β is the temporal growth exponent, and $z = \alpha/\beta$. The parameters α and β are used to classify the scaling of growing surfaces and thereby deduce the combined growth process. We emphasize that different combinations of mechanisms may dominate the surface evolution as growth proceeds leading to different regimes of dynamic scaling and growth behavior.

Surfaces of single crystal or amorphous films have been the focus of most of the previous theoretical and experimental work. While surface scaling in polycrystalline materials[7–12] has been demonstrated, none of these studies has quantified the effects of grain growth and crystallographic texture on roughness and dynamic scaling. For example, grain-boundary grooves contribute to the surface profile, and the grain size may limit the lateral extent of processes acting on individual grain surfaces. In addition, since film crystallographic texture often evolves during growth, structures that depend on mechanisms acting on specific surface crystallographic planes and directions will develop only as grain growth and texture evolution allow. Thus careful grain size and crystallographic characterizations must be considered in order to understand surface evolution. Note that the boundary motions that accomplish grain growth are driven by boundary-curvature–capillary effects, and that the "bulk" film grain growth process is expected to have a significant influence on surface evolution. We characterize in this paper the evolution of surface structures during the growth of polycrystalline Al films by atomic force microscopy and dynamic scaling analysis and incorporate the ef-

0163-1829/2000/61(11)/7692(8)/$15.00 PRB 61 7692 ©2000 The American Physical Society

fects of grain growth. We illustrate that Al grain-growth-induced smoothing during sputter deposition at room temperature results in an initial regime of constant roughness below ≈ 0.3 μm in thickness during which a near-(111) crystallographic texture emerges from an initial nearly randomly oriented film. Above 0.3 μm thickness further deposition is characterized by continued grain growth, a slight but gradual increase in the near-(111) texture component, and roughness evolution described by scaling exponents $\alpha > 1$ and $\alpha \approx 0.35$ at small and intermediate scan lengths, respectively, as measured by power spectral density analysis and image variography. The growth exponent $\beta = 0.55$ as measured with long length scans for films thicker than 0.3 μm. Interestingly, three distinct surface morphologies described as flat grains, hillocks, and ridges emerge in this second regime. The ridges are aligned approximately along $\langle 110 \rangle$ surface directions and are interpreted as Schwoebel-barrier-induced periodic structures that arise due to the vicinal rather than exact (111) orientation of the majority of the Al grains.

EXPERIMENT

A load-locked magnetron sputter system was used to deposit pure Al thin films onto 150-mm-diam thermally oxidized Si(100) substrates using high-purity Ar as the working gas at 2 mTorr pressure. The deposition rate was 1 μm/min and film thicknesses ranging from 0.1 to 1 μm provided samples of the film evolution during growth. The base pressure of the sputter chamber was less than $\sim 2 \times 10^{-8}$ Torr and wafers were outgassed prior to entering the deposition chamber. Substrates were held at near ambient (≈ 25 °C) temperature during deposition by clamping the substrates to the platen through which Ar flow at room temperature was directed onto the substrate backside. Substrate and film self-heating were estimated to be below 20 °C during deposition. The target diameter was 29.2 cm and the stationary substrates were centered directly below the target at a spacing of 4.3 cm. This sputtering geometry ensures an even deposition flux with a substantial oblique directional component across the substrate surface.

Film surface morphology was obtained with an atomic force microscope (AFM) (Digital Instruments Nanoscope III) operated in tapping mode using an etched single-crystal Si tip with a radius of 10 nm. Collected data consisted of height information on square 512×512 arrays of pixels from area scans with lengths from 2 to 15 μm. Surface roughness was characterized by R_{rms} values, which give an average roughness value, and power spectrum density (PSD) analysis, which deconvolutes the roughness as a function of surface lateral length scales. PSD analysis correlates the vertical amplitude with the spatial frequency of surface features and may also reveal characteristics of the surface structure.[13]

In the one-dimensional (1D) case the frequency spectrum of the PSD (1DPSD) is given by

$$\frac{1}{L}\left(\int h(x)e^{i2\pi fx}dx\right)^2 \tag{4}$$

in units of nm^3, where L is the scan length, f is the spatial frequency, x is the fast scan direction of an area scan, and $h(x)$ is the line profile. The 1DPSD spectra were obtained by taking the Fourier transform of individual line scans that comprise an area scan, squaring the amplitude of the Fourier coefficients to determine the ''power,'' and averaging the (512) individual line scan powers at each frequency to generate the 1DPSD. Representative 1DPSD plots are obtained by cropping together spectra from the different scan lengths in order to evenly account for spatial features over a wide range of length scales.

The scaling behavior of surfaces can be analyzed from their power density spectra.[14,15] In a finite frequency range, a self-affine structure exhibits a power-law decay

$$1\mathrm{DPSD}(f) = K_0 f^{-\gamma}, \tag{5}$$

where K_0 is a constant dependent on the system and γ is related to the scaling exponent (α) by $\alpha = (\gamma - d)/2$,[16] where the line scan dimension $d = 1$.

We have also investigated the scaling properties of the surface based on single-image and multiple-image variography (Ref. 1, p. 302.) The R_{rms} values for different areas were determined from nonoverlapping windows covering the original micrographs. The growth exponent β and scaling exponent α were obtained from Eqs. (2), (3), and (5).

Grain size and morphology were determined by plan view and cross-section transmission electron microscopy (TEM). Approximately 500 grains per film condition were measured to determine median grain sizes and distributions. Film crystallographic texture was determined by the x-ray diffraction pole figure method (XPF) and subsequent analysis to quantitatively determine the volume fractions of each texture component at each thickness. (Reference 17 provides a more detailed summary of the TEM and XPF methods and results.) The local crystallographic orientation of individual grains was obtained using the orientation imaging microscopy (OIM) method[18] in a scanning electron microscope by indexing electron backscattered diffraction patterns from selected submicrometer-sized regions of interest.

RESULTS

The images in cross-section (Fig. 1) and plan-view (Fig. 2) TEM illustrate that the Al grains maintain a columnar morphology as grain growth proceeds throughout deposition. This self-similar ''normal grain-growth'' process is therefore accomplished by the motion of the grain boundaries through the film rather than preferential growth of grains at the surface. The size-competitive grain-growth mechanism is driven primarily by (capillary) boundary-curvature forces and maintains an apparent log-normally distributed size population.[17] The mean grain size $\langle d \rangle$ increases with thickness as

$$\langle d \rangle \approx (kt)^n \approx (k'h)^{0.9}, \tag{6}$$

where k and k' are thermally activated kinetic rate constants, t is the deposition time, and h is the film thickness, and we assume a constant deposition rate. Obviously the exponent n is required in order to determine the grain-growth activation energy. Note also that $\langle d \rangle$ accurately represents the in-plane grain size due to the columnar grain morphology, Fig. 1. Under growth conditions where boundary motions are restricted, grain competition for arriving flux at the growing surface will also drive coarsening with growth of noncolum-

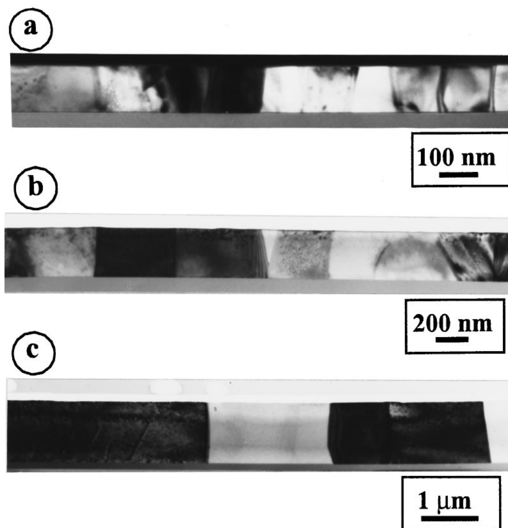

FIG. 1. Cross-section TEM images of (a) 0.1-μm, (b) 0.3-μm, and (c) 1-μm-thick films showing that a columnar morphology is maintained during film growth.

nar tapered grains with median size $\langle d_s \rangle$ *at the surface* proportional to $(t)^{0.5}$ and $(h)^{0.5}$.[19]

Analysis of the XPF results showed two components of film texture, one that is randomly oriented and one comprised of grains whose out-of-plane [111] direction is near to but not exactly aligned with the film normal direction. Al films with vicinal (111) grain surfaces forming a primary near-(111) texture have been previously observed when similarly deposited on amorphous substrates.[20] The volume fraction of the near-(111) component rises with thickness from $\approx$0.53 at 0.1 μm, to 0.85 at 0.3 μm and to $\approx$0.95 at 1.0 μm.[17] The near-(111) texture peak offset decreases slightly with thickness, from about 9° from the film normal at 0.1 μm to 5° from the film normal in the 1.0-μm film. The primary near-(111) texture component develops during deposition as a result of grain growth in which surface and interfacial energy minimization provide an additional driving force for the preferential growth of the near-(111) oriented grains.[17]

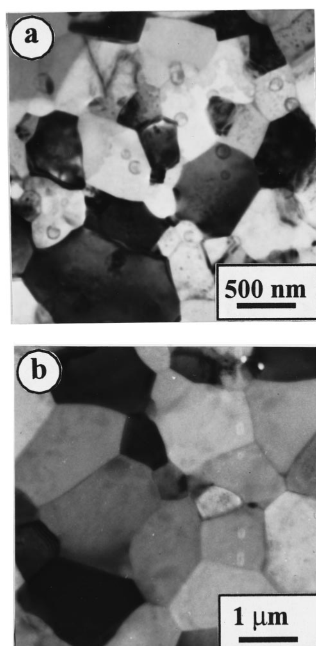

FIG. 2. Plan-view TEM micrographs of (a) 0.3-μm and (b) 1-μm-thick films. The grains are columnar and their size increases with thickness.

The surface morphology of the 0.1-, 0.3-, 0.6- and 1-μm-thick films is shown in Fig. 3. As growth proceeds the surface develops distinct features identified as growth hillocks, grain-boundary grooves, nominally flat grains, and grains with periodic ridge features. Note the close correlation between the nominal grain size, Fig. 2, and the regions of consistent surface morphology, Fig. 3. The hillocks are randomly scattered, while the ridges have spacing smaller than the grain size but extend uniformly over the surface of individual grains. Similar morphologies were found on all films thicker than 0.3 μm, with the ridge and hillock features missing below this thickness.

The R_{rms} values obtained from 2 μm$\times$2 μm AFM area scans indicate relatively smooth surfaces and two regimes of R_{rms} variation with thickness. R_{rms} is nearly constant or slightly decreasing for films less than 0.3 μm thick but monotonically increases with thickness thereafter (Fig. 4). The error bars in Fig. 4 result from the averaging of typically 10 area scans. The overall R_{rms} dependence on film thickness yields a growth exponent $\beta = 0.41$; however, we obtain $\beta = 0.55$ using only R_{rms} values from films greater than 0.3 μm thick. The constant roughness during the early stages of film formation can be explained as the result of grain growth, discussed below.

The 1DPSD spectra (Fig. 5) exhibit several distinct regions, a frequency-independent roughness at low frequency (long length scales), and a frequency-dependent region at higher frequency (short length scales.) Interestingly, for the films thicker than 0.2 μm, Figs. 5(b)–5(d), this higher-frequency behavior is composed of two constant-slope regions with different scaling exponents, implying two combinations of processes acting to develop the surface morphologies during growth. The scaling exponents were extracted from the two constant-slope 1DPSD regions based on Eq. (5). For the higher-frequency region $\alpha_{\mathrm{I}} = 1.36 \pm 0.09$, while for the intermediate self-affine region $\alpha_{\mathrm{II}} = 0.30 \pm 0.03$.

These scaling exponents are similar to previous theoretical results that have identified two types of growth-front dynamic scaling behavior. The first type has a self-affine and time-invariant growth morphology characterized by a scaling exponent $0 < \alpha < 1$. This behavior has been described as a balance between roughening mechanisms, such as random fluctuations in the depositing flux, and smoothing processes, such as diffusion at the growth front so that the local structure remains unchanged.[1,6] For example, $\alpha = 0.39$ and $\beta = 0.25$ are the predicted values for the scaling and growth exponent in the nonlinear Kardar-Parisi-Zhang (KPZ) model.[2] The second type is anomalous dynamic scaling, which gives $\alpha \geqslant 1$.[4,21] In this situation the roughening fluctuations and the smoothing effects cannot quite reach a balance, and the local surface slope increases with time. For example, in the linear diffusional model[4] the predicted values are $\alpha = 1.4$ and $\beta = 0.36$. We suggest that in our case, the intermediate-frequency self-affine region corresponds to the

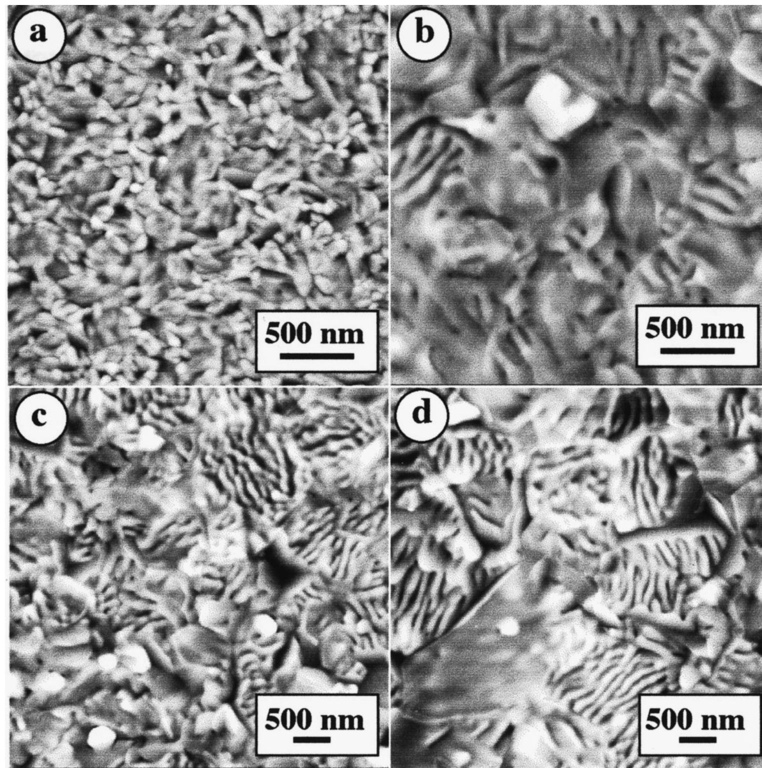

FIG. 3. (a) AFM topographic images of Al thin films with thickness (a) 0.1 μm and height scale $z=40.0$ nm, (b) 0.3 μm, $z=60.0$ nm, (c) 0.6 μm, $z=60.0$ nm, and (d) 1 μm, $z=80.0$ nm. For films thicker than 0.3 μm, (b)–(d), different features develop on the surface of the film: hillocks, and boundary grooves.

KPZ dynamic scaling behavior, while the high-frequency region is characterized by anomalous dynamic scaling behavior dominated by surface diffusion.

The frequencies of transition, marked by arrows in Fig. 5, between the various regimes of 1DPSD behavior are of interest since they infer correlation lengths or other physically meaningful characteristic length scales. The first characteristic dimension (CD_I) is defined by the (inverse) frequency of transition between the high-frequency and self-affine intermediate-frequency regions. The CD_I values extracted at points of 1 DPSD slope change are approximately constant with thickness (Table I) and are equal to the periodic ridge spacing determined from the average peak-to-peak ridge separation from cross-section surface profiles. The average ridge spacing (obtained from films $\geqslant$0.3 μm thick) is 110 $\pm$5 nm. The ridge spacing and CD_I therefore represent the transition between the linear surface-diffusion-dominated regime ($\alpha_I = 1.36 \pm 0.09$) and the nonlinear growth mode region ($\alpha_{II} = 0.30 \pm 0.03$).

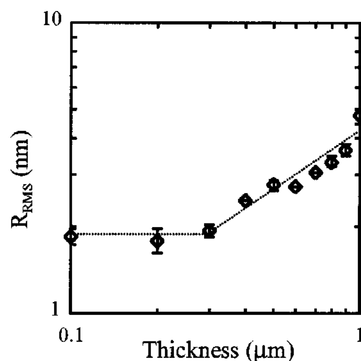

FIG. 4. Average surface roughness (R_{rms}) variation with film thickness displays an early regime in which R_{rms} is constant and a later regime $\geqslant$0.3 μm thickness in which R_{rms} increases as $\approx h^{0.55}$.

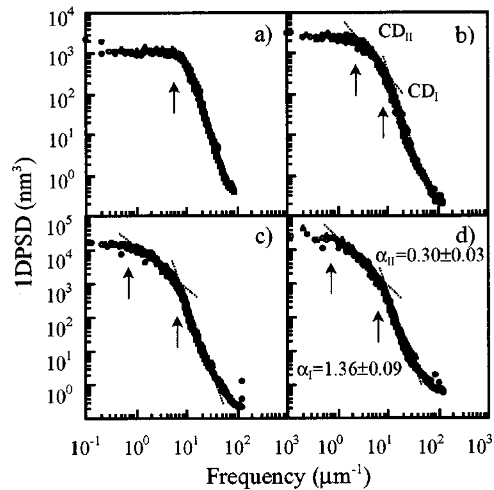

FIG. 5. Power spectral density vs spatial frequency for (a) 0.1-μm, (b) 0.3-μm, (c) 0.6-μm, and (d) 1-μm-thick films illustrating different regimes of surface roughness. For (a) there is a frequency-independent regime at low frequency and a constant-slope regime at higher frequencies, whereas for thicker films (b)–(d) there are two constant-slope regimes at intermediate and high frequencies. The transitions between the roughness regimes define the characteristic dimensions CD_I and CD_{II} that represent the ridge spacing and grain size, respectively. The roughness exponents for the two constant slope regimes are displayed in (d).

TABLE I. Correlation lengths estimated from both PSD plots and image variograms.

	PSD		Image variography	
Thickness (μm)	CD_I (nm)	CD_{II} (nm)	CD_I (nm)	CD_{II} (nm)
0.1		125		100
0.3	123	455	107	333
0.6	112	573	111	582
1	110	1100	125	1000

Similarly, a second characteristic dimension (CD_{II}) indicates the transition between the low-frequency random roughness plateau and the intermediate-frequency self-affine region in the 1DPSD. The CD_{II} values increase with thickness and are listed in Table I. Previously we have shown that CD_{II} corresponds well to the accurately determined median grain size in each film.[17] The low-frequency randomly rough behavior suggests that in this region there is no correlation along the surface at these length scales (inverse frequencies) as growth proceeds. We interpret the transition between these regimes as evidence of the polycrystalline nature of the films, with grain size defining this transition.

Image variography was also used to extract the scaling exponents and the correlation lengths. Figure 6 shows variograms of surface roughness as a function of scan lengths for films 0.1, 0.3, 0.6, and 1 μm thick. Evident in films $\geqslant 0.3$ μm thick are two constant-slope regions and a flat plateau, similar to the 1DPSD results. The scaling exponents based on Eq. (3) extracted from the nonplateau regions of the variograms are $\alpha_I = 1.17 \pm 0.13$ and $\alpha_{II} = 0.38 \pm 0.05$ at small and intermediate scan lengths, respectively. Correlation lengths separating the three constant-slope regions were also extracted and compared with the values found from the PSD plots, Table I. The values are in excellent agreement, indicating

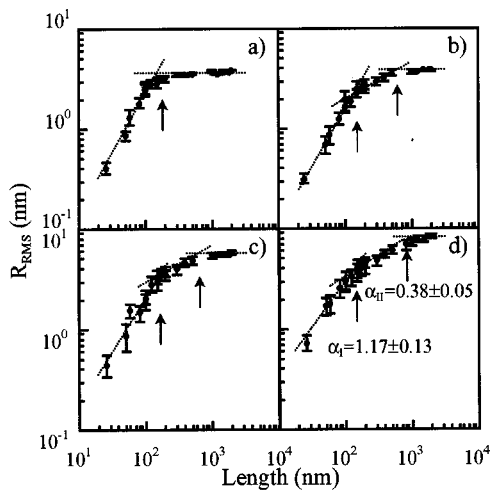

FIG. 6. Variograms of interface widths ($R_{\rm rms}$) vs window length for (a) 0.1 μm, (b) 0.3 μm, (c) 0.6 μm, and (d) 1 μm film thickness. Different roughness regimes are identified and separated by correlation lengths obtained at points of slope change marked by the arrows in the figures. The roughness exponents for the two constant-slope regimes are displayed in (d). Each point represents the average of 20–30 measurements.

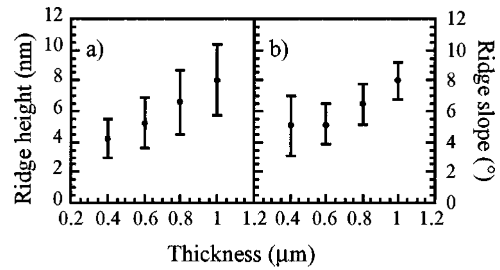

FIG. 7. (a) Average peak-to-valley ridge height increases with film thickness; (b) ridge slope determined as the ratio of ridge height to width also increases during film growth. The error bars primarily reflect the distribution in ridge height and width.

that both methods yield consistent scaling exponents characterizing two regimes of growths as well as the characteristic lengths of transition between them.

We now focus on the periodic ridge features with spacing equal to CD_I's, which mark the transition from the linear surface-diffusion-dominated region to one whose growth mode is controlled by nonlinear terms. Roberts and Dobson[22] reported similar surface features for pure Al films grown by evaporation on oxidized Si substrates. They briefly refer to these features as effects of preferential condensation. Cross-section AFM profiles show that ridges grow in height but maintain a constant periodicity during deposition. Figures 7(a) and 7(b) illustrate that the average peak-to-valley height and the average slope increase with film thickness, respectively. A cross-section TEM of a ridged grain, Fig. 8, illustrates that the ridges are actually very gentle ''hills'' on the surface that may not be apparent in the enhanced height contrast AFM images, Fig. 3.

The ridge arrays maintain the same direction over areas comparable to the grain size, Figs. 3(b)–3(d), but vary in alignment on different grains. This is consistent with a specific crystallographic ridge direction within each grain but a random grain-to-grain in-plane orientation. Since the OIM method provides local crystallographic orientation, specific out-of-plane orientations for both ''flat'' grains and ridged grains as well as the crystallographic ridge direction within individual grains were measured. Of the approximately 100 grains characterized by OIM, virtually all grains in a 1.0-μm film were oriented with the [111] direction between 5° and

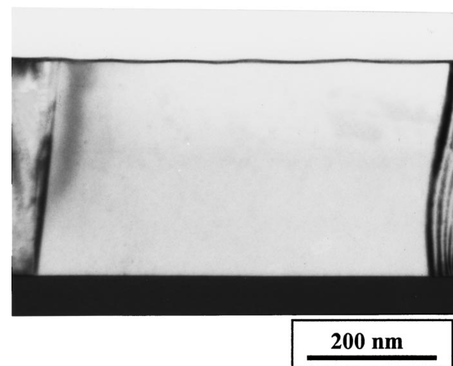

FIG. 8. Cross-section TEM of 0.3-μm-thick film showing a grain with the ridge features on top. The ridge height is on the order of several nanometers as shown in Fig. 7 with a lateral spacing of $\approx$110 nm.

8° from the exact film normal, consistent with the x-ray results. However, analysis of approximately 50 ridged grains showed consistent ridge alignment along a [110] direction on an individual grain surface with an average misorientation of 6° from the exact [110] direction.

DISCUSSION

Film-deposition conditions are critical factors that determine the grain-size effect on surface scaling and evolution. The rate of thermally activated grain growth depends on the homologous deposition temperature as well as factors such as the deposition rate, contamination, and second phase particles. Typically, the grain growth kinetic exponent (n) varies from 0 to 1.0, with the lower value approached at very low homologous temperatures such that limited atomic mobility prevents grain competition at the surface or by boundary motion. Fibrous film morphologies are thus proposed under such conditions.[23] At higher temperatures, atomic and boundary mobilities allow for grain competition during deposition. If grain growth (via boundary motion) is rapid enough then the film may maintain the ''film-thickness limit'' grain size,[24] with $\langle d \rangle$ proportional to $t^{1.0}$ and $h^{1.0}$, as deposition proceeds.

We propose that the extensive grain growth in our Al films during deposition at $T/T_m = 0.34$, with $n = 0.9$, accounts for the significant smoothing component during film growth from 0.1 to 0.3 μm. Several mechanisms are described that provide smoothing early in the film growth. For example, significant reduction in the roughness occurs as hemispherical or irregularly shaped discrete grain islands grow to impingement as the film achieves continuity, forming grain boundaries and grooves. Recent results[25] obtained as AlCu films achieve continuity between 10 and 100 nm in thickness confirm both this smoothing effect and its persistence for some period beyond film continuity as grain growth continues during deposition.

Second, consider the significant boundary groove contribution to the surface profile in the thin-film, small-grain-size limit. The disappearance of grooves as grains are eliminated will depend explicitly on the rate of grain growth as deposition proceeds. Thus with limited grain growth relatively few grains and boundary grooves are removed, whereas the rapid grain growth exhibited here ($n = 0.9$) results in significant groove elimination and smoothing. Finally, consider the increase in the fraction of grain surfaces with near (111) orientation from ≈ 0.53 to ≈ 0.85 during film growth from 0.1 to 0.3 μm. The resulting increased alignment of (111) surface facets with the film growing plane could easily lead to a roughness decrease in this early regime.

There are previous reports of surface smoothing presumably due to grain growth under various film conditions. Gimzewski *et al.*[26] observed a roughness decrease as Ag films deposited at 90 K were brought to ''warmer'' conditions, and discussed an apparent increase in (presumed) grain size. Douketis *et al.*[9] observed decreased roughness in Ag films deposited at 300 K ($T/T_m = 0.24$) as compared to 100-K films ($T/T_m = 0.08$), and a roughness decrease in Ag films deposited at 300 K and subsequently annealed at 560 K. Wei *et al.*[27] observed a roughness minimum for depositions at 773 K ($T/T_m = 0.38$) in $\approx$ 100-nm-thick Pt films deposited between 300 and 1073 K. Interestingly, Chiarello *et al.*[7(f)] also observed a constant-roughness regime early during Au film growth under conditions (300 K, $T/T_m = 0.22$, low deposition rate) that enhance grain-growth effects, whereas a monotonic roughness increase was observed at 220 K and at a higher deposition rate. Thus we propose grain growth as an effective mechanism for smoothing during deposition. This smoothing contribution is expected to continue as the texture is being developed and until the grain size is somewhat longer than other length scales characteristic of surface-active processes, i.e., until $\langle d \rangle$ is greater than $\approx 2-3$ CD_I for our Al films. In this regime, for $h \leqslant 0.3$ μm, we find $\beta \approx 0$, whereas for $h \geqslant 0.4$ μm we find $\beta = 0.55$. These temporal scaling exponents were similarly observed by Chiarello *et al.*[7(f)] for the $T/T_m = 0.22$ low-deposition-rate Au films.

We may speculate about the deposition conditions that govern the transition (in film thickness) between an early grain-growth-induced smoothing regime and subsequent roughening. The homologous temperature should be large enough ($T/T_m \geqslant 0.2$) to allow for boundary motions but below that which allows significant bulk atomic mobility ($T/T_m \leqslant 0.5$), while the deposition rate should be low enough to allow for reasonable boundary motions during thickening. More detailed modeling would include flux directionality (oblique during sputtering versus collimated during evaporation), substrate chemistry (nucleation rate effects on film continuity),[25] and contamination as necessary factors.

Ridges and growth hillocks appear in the later temporal regime, $\beta \approx 0.55$. We note that CD_I (and the constant ridge spacing) defines the transition between the linear surface-diffusion-dominated regime and the nonlinear growth mode regime. Thus the ridge spacing indicates the spatial limit of structures that can be eliminated by local surface diffusion. This was corroborated by comparison to a model for the stability of surface perturbations during film growth.[28] In that model a temperature-dependent effective surface diffusion length λ_0 is defined by the balance of shadowing effects during deposition and the surface-tension-driven smoothing effects of surface diffusion. Identification of our CD_I or ridge spacing as λ_0 yield surface diffusivities and activation energies consistent[17] with published data for Al.[29]

Grain-size effects persist even as $\langle d \rangle$ grows beyond $\approx 2-3$ CD_I since the grain size limits the extent of correlated surface processes. That is, correlated evolution may extend across the surface of a (crystal) grain similarly among the many grains, but may not extend to adjacent grains. In our films the ridge arrays are thus aligned on individual grains but vary in surface alignment from grain to grain. In another example, the roughness associated with shadowing-induced hillock growth is limited in the lateral extent by the hillock, i.e., the grain size, which, however, increases during growth. Therefore we identify the median grain size (and CD_{II}) as defining the length scale below which correlated surface evolutions occur and above which randomly rough surfaces evolve in our polycrystalline thin films. We further suggest that an analogous grain-size effect similarly defines the transition length scale between correlated and uncorrelated surface development in deposited organic[14,15] and amorphous[30] films. The organization of polymers into domains, and domains of fully-dense amorphous material separated by low-density or voided regions, may serve as the respective grain-

equivalent domains in these materials.

Others[7,8,10–12,26,27] have interpreted apparent grain-size effects as influencing surface evolution using, however, estimated grain or column sizes from surface topologies or x-ray methods. While those conclusions cannot be disputed we note that such methods, especially the surface topological estimations, provide only rough approximations for the actual grain size and morphology. As an example, Zubimendi[8(d)] estimated the different size of columns and ''domains of facets'' as they varied in relative population for deposition temperatures $T/T_m \geqslant 0.35$ without identifying the actual crystallite size.

Since the crystallographic orientation of the growing surface is critical, quantitative measurement of the film texture as it evolves during deposition is necessary for full understanding of surface evolutionary processes. For example, the texture of Ag films deposited on glass substrates was found to vary[31] between (111) and (100) primary textures as a function of thickness and temperature. However, the widely used θ–2θ x-ray method provides only a qualitative estimate of film texture. Jeffries, Zuo, and Craig[10] observed both (111) and (100) peaks with the θ–2θ method which normally indicates a largely random texture rather than their ''two kinds of crystallites [(111) and (100)]'' conclusion. Our quantitative results show that the development and optimization of the Al(111) texture from a nearly random film correlate well with the smoothing effect during growth.

Previous reports have shown two spatial dynamic scaling regimes similar to the $\alpha_{\mathrm{I}}=1.17-1.36$ and $\alpha_{\mathrm{II}}=0.30-0.38$ found for our sputtered Al films. In general those reports found $\alpha_{\mathrm{I}}\approx 0.89-0.95$ and $\alpha_{\mathrm{II}}\approx 0.35-0.49$ in Au films evaporated onto glass substrates at T/T_m between 0.22 and 0.43,[8(a),8(d),8(e)] electrodeposited Au at $T/T_m=0.22$,[8(c)] and $LiCoO_x$ films sputter deposited onto Ni substrates.[12] We similarly conclude that region I is described by the linear diffusional model[4] with a predicted value $\alpha_{\mathrm{I}}=1.4$ in which roughening fluctuations and surface diffusion smoothing effects are not balanced, leading to a local surface slope increase as in anomalous dynamic scaling.[4,21,30] Region II, with $\alpha_{\mathrm{II}}\approx 0.35$, is characterized by balance between shadowing-induced roughening and longer-range diffusional processes so that the local structure remains unchanged,[1,6] in agreement with the $\alpha=0.39$ scaling exponent predicted by the nonlinear KPZ model.[2]

In terms of mechanisms for ridge formation, interesting features of fcc (111) surfaces are the two types of close-packed steps with formation energies that are about half of that required to create the surface.[29] The steps orient along ⟨110⟩-type directions and are typically labeled according to their {111} or {100} microfacets.[29] Their different geometries lead to different formation energies, diffusion mechanisms, and energy barriers that in turn have different implications for crystal growth. The growth shapes predicted can be fractal, triangular, or hexagonal depending on the temperature[32] and have been observed in fcc single crystals[33] and as mounds in polycrystalline[11] Pd films. We now refer to the single-crystal study in order to analyze surface evolution within the grains in our polycrystalline Al films. The grain surfaces are primarily vicinal (111) and show periodic ridge features oriented along ⟨110⟩-type directions. We believe that these ridges form due to spontaneous ⟨110⟩ step formation on the vicinal (111) surfaces, with their growth induced by Schwoebel-barrier mechanism.[34] Rather than slope selection[35] our increase in the ridge height and slope during film growth may be explained by the increased shadowing effects of the noncollimated sputter deposition flux. This slope and height increase suggest that the sides of each individual ridge are not facets but are comprised of ⟨110⟩ ledges separated by (111) terraces. If we consider perfectly (111)-oriented but ridged grains with evenly spaced ledges along ridge sides, we find the distance between ledges to be 27 Å for a 5° slope as in the 0.3-μm-thick film. As the slope increases to 8° (in the 1-μm film) the ledge separation decreases to ≈17 Å. The limited AFM resolution does not allow more detailed characterization of the ridge structure; however, we expect somewhat smaller ledge spacing on ridge slopes for the vicinal (111)-oriented grains.

Of the three ⟨110⟩-type directions on Al(111) surfaces only one of them is selected by the periodic ridges. The threefold (111) surface symmetry is broken by the vicinal ⟨111⟩ grain orientation as determined from XPF and OIM diffraction results. These surfaces result from the near-(111) texture, and lead to ridges oriented along a ⟨110⟩ direction when the [111] tilt from exact film normal is about a ⟨110⟩ surface direction. However, we propose that no surface ridges form when the rotation of the out-of-plane [111] grain direction is about an arbitrary axis, thereby rationalizing the existence of grains with smooth nonridged surfaces. Future surface scanning tunneling microscopic characterization may resolve the atomic level detail of these ridge structures.

CONCLUSIONS

We report the observation of dynamic scaling for polycrystalline Al films sputter deposited on amorphous substrates. Temporal regimes of early surface smoothing followed by roughening are explained by the effects of grain-boundary grooves and grain growth during deposition. Quantitative film texture characterization illustrates the development of a vicinal (111) texture that evolves from a nearly random texture as deposition proceeds above 0.1 μm in thickness.

The spacing of ridge structures and the well-characterized median grain size correspond to characteristic dimensions that define transitions between regimes of combinations of physical processes responsible for surface evolution. The two dynamic scaling exponents were consistently determined by both PSD and image variography analyses. We found a surface-diffusion-dominated anomalous scaling growth mode at short length scale and a nonlinear KPZ-type mode at longer length scale.

Periodic ridges form along ⟨110⟩ directions on vicinal (111)-oriented grains and are due to spontaneous development and growth of steps along ⟨110⟩ directions induced by the Schwoebel-barrier mechanism. We attribute the formation of the ridges along a particular [110] direction as opposed to all three ⟨110⟩ as due to the vicinal (111) surface orientation, offset by ≈6° from exact [111] texture.

[1] A. L. Barabasi and H. E. Stanley, *Fractal Concepts in Surface Growth* (Cambridge University Press, Cambridge, 1995).
[2] M. Kardar, G. Parisi, and Y.-C. Zhang, Phys. Rev. Lett. **56**, 889 (1986).
[3] S. F. Edwards and D. R. Wilkinson, Proc. R. Soc. London, Ser. A **381**, 17 (1982).
[4] D. E. Wolf and J. Villain, Europhys. Lett. **13**, 389 (1990).
[5] Z.-W. Lai and S. Das Sarma, Phys. Rev. Lett. **66**, 2348 (1991).
[6] F. Family and T. Vicsek, J. Phys. A **18**, 75 (1985).
[7] (a) J. Krim, D. H. Solina, and R. Chiarello, Phys. Rev. Lett. **66**, 181 (1991); (b) R. P. Chiarello, V. Panella, and J. Krim, *ibid.* **67**, 3408 (1991); (c) H. You, R. P. Chiarello, H. K. Krim, K. G. Vandervoort, and C. Thompson, *ibid.* **70**, 2900 (1993); (d) J. Krim, I. Heyvaert, C. Van Haesendonck, and Y. Bruynseraede, *ibid.* **70**, 57 (1993); (e) C. Thompson, G. Palasantzas, Y. P. Feng, S. K. Sinha, and J. Krim, Phys. Rev. B **49**, 4902 (1994); (f) R. P. Chiarello, H. You, H. K. Kim, T. Roberts, R. T. Kempwirth, D. Miller, K. E. Gray, K. G. Vandervoort, N. Trivedi, S. R. Philpot, Q. J. Zhang, S. Williams, and J. B. Ketterson, Surf. Sci. **380**, 245 (1997).
[8] (a) R. C. Salvarezza, L. Vasquez, P. Herrasti, P. Ocon, J. M. Vara, and A. J. Arvia, Europhys. Lett. **20**, 727 (1992); (b) P. Herrasti, P. Ocon, L. Vasquez, R. C. Salvarezza, J. M. Vara, and A. J. Arvia, Phys. Rev. A **45**, 7440 (1992); (c) L. Vasquez, R. C. Salvarezza, P. Ocon, P. Herrasti, J. M. Vara, and A. J. Arvia, Phys. Rev. E **49**, 1507 (1994); (d) J. L. Zubimendi, M. E. Vela, R. C. Salvarezza, L. Vasquez, J. M. Vara, and A. J. Arvia, *ibid.* **50**, 1367 (1994); (e) L. Vazquez, R. C. Salvarezza, P. Herrasti, P. Ocon, J. M. Vara, and A. J. Arvia, Surf. Sci. **345**, 17 (1996).
[9] C. Douketis, Z. Wang, T. L. Haslett, and M. Moskovits, Phys. Rev. B **51**, 11 022 (1995).
[10] J. H. Jeffries, J.-K. Zuo, and M. M. Craig, Phys. Rev. Lett. **76**, 4931 (1996).
[11] I. B. Chung and Y. M. Koo, J. Appl. Phys. **86**, 306 (1999).
[12] M. U. Kleinke, J. Davalos, C. Polo da Fonseca, and A. Gorenstein, Appl. Phys. Lett. **74**, 1683 (1999).
[13] M. W. Mitchell and D. A. Bonnell, J. Mater. Res. **5**, 2244 (1990).
[14] F. Biscarini, P. Samori, O. Greco, and R. Zamboni, Phys. Rev. Lett. **78**, 2389 (1997).
[15] G. W. Collins, S. A. Letts, E. M. Fearon, R. L. McEachern, and T. P. Bernat, Phys. Rev. Lett. **73**, 708 (1994).
[16] R. F. Voss, in *Scaling Phenomena in Disordered Systems*, edited by R. Pynn and A. Skejeltorp (Plenum, New York, 1985), pp. 1–11.
[17] A. E. Lita and J. E. Sanchez, Jr., J. Appl. Phys. **85**, 876 (1999).
[18] B. L. Adams, S. I. Wright, and K. Kunze, Metall. Trans. A **24**, 819 (1993).
[19] A. J. Dammers and S. Radelaar, Mater. Sci. Forum **94-96**, 345 (1991).
[20] D. B. Knorr, in *Materials Reliability in Microelectronics III*, edited by K. P. Rodbell, W. F. Filter, H. J. Frost, and P. S. Ho, MRS Symposia Proceedings No. 309 (Materials Research Society, Pittsburgh, 1993), p. 75.
[21] J. G. Amar, P.-M. Lam, and F. Family, Phys. Rev. E **47**, 3242 (1993); T.-M. Lu, H.-N. Yang, and G.-C. Wang, in *Fractal Aspects of Materials*, edited by F. Family, P. Meakin, B. Sapoval, and R. Wool, MRS Symposia Proceedings No. 367 (Materials Research Society, Pittsburgh, 1995), p. 283.
[22] S. Roberts and P. J. Dobson, Thin Solid Films **135**, 137 (1986).
[23] B. A. Movchan and A. V. Demchishin, Fiz. Met. Metalloved. **28**, 653 (1969).
[24] W. W. Mullins, Acta Metall. **6**, 414 (1958).
[25] A. E. Lita and J. E. Sanchez, Jr. (unpublished).
[26] J. K. Gimzewski, A. Humbert, J. G. Bednorz, and B. Reihl, Phys. Rev. Lett. **55**, 951 (1985).
[27] S. Wei, B. Li, T. Fujimoto, and I. Kojima, Phys. Rev. B **58**, 3605 (1998).
[28] D. J. Srolovitz, A. Mazor, and B. G. Bukiet, J. Vac. Sci. Technol. A **6**, 2371 (1988).
[29] R. Stumpf and M. Scheffler, Phys. Rev. Lett. **72**, 254 (1994).
[30] H.-N. Yang, Y.-P. Zhao, G.-C. Wang, and T.-M. Lu, Phys. Rev. Lett. **76**, 3774 (1996).
[31] A. Gittis and D. Dobrev, Thin Solid Films **130**, 335 (1985).
[32] R. Stumpf and M. Scheffler, Phys. Rev. B **53**, 4958 (1996).
[33] M. Kalff, G. Comsa, and T. Michely, Phys. Rev. Lett. **81**, 1255 (1998).
[34] R. L. Schwoebel and E. J. Slipsey, J. Appl. Phys. **37**, 3682 (1966); R. L. Schwoebel, *ibid.* **40**, 614 (1969).
[35] M. Siegert and M. Plischke, Phys. Rev. Lett. **73**, 1517 (1994).